




# Prototype early diagnostic model for invasive pulmonary aspergillosis based on deep learning and big data training

Wei Wang<sup>1,2</sup>  | Mujiao Li<sup>1,3</sup> | Peimin Fan<sup>4</sup> | Hua Wang<sup>5</sup>  | Jing Cai<sup>5</sup>  | Kai Wang<sup>5</sup> | Tao Zhang<sup>6</sup> | Zelin Xiao<sup>7</sup> | Jingdong Yan<sup>6</sup> | Chaomin Chen<sup>1</sup> | Qingwen Lv<sup>2</sup>

<sup>1</sup>School of Biomedical Engineering, Southern Medical University, Guangzhou, China

<sup>2</sup>Department of Information, Zhujiang Hospital, Southern Medical University, Guangzhou, China

<sup>3</sup>Department of Information, Guangzhou First People's Hospital, Guangzhou, China

<sup>4</sup>Department of Information Center, Guangzhou Chest Hospital, Guangzhou, China

<sup>5</sup>Department of Critical Care Medicine, Zhujiang Hospital, Southern Medical University, Guangzhou, China

<sup>6</sup>Department of Information, Nanfang Hospital, Southern Medical University, Guangzhou, China

<sup>7</sup>Department of Surgery, Guangzhou Chest Hospital, Guangzhou, China

## Correspondence

Jingdong Yan, Department of Information, Nanfang Hospital, Southern Medical University, Guangzhou 510515, China.  
Email: [jdyan@smu.edu.cn](mailto:jdyan@smu.edu.cn)

Chaomin Chen, School of Biomedical Engineering, Southern Medical University, Guangzhou 510515, China.  
Email: [gzcmm@smu.edu.cn](mailto:gzcmm@smu.edu.cn)

Qingwen Lv, Department of Information, Zhujiang Hospital, Southern Medical University, Guangzhou 510282, China.  
Email: [gzbeer@smu.edu.cn](mailto:gzbeer@smu.edu.cn)

## Funding information

National Key R&D Program of China, Grant/Award Number: 2019YFC0118805; Clinical Research Startup Program of Southern Medical University; Guangdong Provincial Department of Education, Grant/Award Number: LC2016PY036

## Abstract

**Background:** Currently, the diagnosis of invasive pulmonary aspergillosis (IPA) mainly depends on the integration of clinical, radiological and microbiological data. Artificial intelligence (AI) has shown great advantages in dealing with data-rich biological and medical challenges, but the literature on IPA diagnosis is rare.

**Objective:** This study aimed to provide a non-invasive, objective and easy-to-use AI approach for the early diagnosis of IPA.

**Methods:** We generated a prototype diagnostic deep learning model (IPA-NET) comprising three interrelated computation modules for the automatic diagnosis of IPA. First, IPA-NET was subjected to transfer learning using 300,000 CT images of non-fungal pneumonia from an online database. Second, training and internal test sets, including clinical features and chest CT images of patients with IPA and non-fungal pneumonia in the early stage of the disease, were independently constructed for model training and internal verification. Third, the model was further validated using an external test set.

**Results:** IPA-NET showed a marked diagnostic performance for IPA as verified by the internal test set, with an accuracy of 96.8%, a sensitivity of 0.98, a specificity of 0.96 and an area under the curve (AUC) of 0.99. When further validated using the external test set, IPA-NET showed an accuracy of 89.7%, a sensitivity of 0.88, a specificity of 0.91 and an AUC of 0.95.

**Conclusion:** This novel deep learning model provides a non-invasive, objective and reliable method for the early diagnosis of IPA.

## KEYWORDS

artificial intelligence, computed tomography, deep learning, invasive pulmonary aspergillosis, predictive medicine, retrospective study

## 1 | INTRODUCTION

The incidence of invasive pulmonary aspergillosis (IPA) has increased dramatically during the past two decades, owing to the widespread use of broad-spectrum antibiotics, systemic administration of glucocorticoids and immunosuppressants, and the increased number of immunocompromised patients with haematological malignancies, solid organ transplantations, diabetes mellitus and acquired immunodeficiency syndrome. The widespread application of chemoradiotherapy and molecular targeted therapy has also played a role in the high prevalence of IPA.<sup>1</sup> The gold standard for IPA diagnosis is exclusively pathological examination; however, only 12%–60% of patients were diagnosed pre-mortem owing to the difficulty of invasive specimen sampling.<sup>2</sup> Currently, recommendations by guidelines for the diagnosis of IPA are mainly based on a comprehensive analysis of host factors, chest computed tomography (CT) image findings and microbiologic evidence, and diagnoses of IPA are classified into proven, probable and possible categories, along with a graded therapeutic strategy.<sup>3,4</sup> Although this strategy is clinically applicable, it largely depends on individual experience and the subjective judgement of the attending physician or radiologist, resulting in a high misdiagnosis rate and a subsequent in-hospital mortality rate of 30%–60%.<sup>5</sup>

Pre-emptive therapy confers morbidity and mortality advantages in the patient population with IPA, arousing an urgent need for a non-invasive, objective and easy-to-use method for early diagnosis.<sup>6</sup> The deep learning algorithm is an important method of artificial intelligence, which extracts advanced abstract features from clinical information and medical images through a hierarchical neural network, achieving automatic diagnosis through self-learning. Existing studies have shown that the deep learning algorithm can improve diagnostic accuracy in conditions such as skin cancer, liver disease, colon cancer, brain tumour, lung cancer, pneumonia and coronavirus disease (COVID-19).<sup>7–14</sup> Given the important role of chest CT images and clinical characteristics in the diagnosis of IPA, for the first time, we constructed a prototype deep learning model for the early diagnosis of IPA, and verified the diagnostic performance of the model internally and externally.

## 2 | MATERIALS AND METHODS

### 2.1 | Patient enrolment and grouping

This project was implemented at two teaching hospitals of Southern Medical University and one specialised chest hospital in Guangzhou, China. The authors confirm that the ethical policies of the journal, as noted on the journal's author guidelines page, have been adhered to and the appropriate ethical review committee approval has been received from the hospital medical research ethics committees. The need for written informed consent was waived given the retrospective nature of the study.

We queried patient data associated with IPA from 1 January 2012 to 30 June 2021 at the three hospitals through the Electronic Medical Record System (eMRS), and manually reviewed the outcomes of histopathological examination. We enrolled patients who met all the following inclusion criteria: (1) age  $\geq 18$  years; (2) invasive syndromes of *Aspergillus* and radiographic abnormalities; (3) typically dichotomous and septate hyphae present on microscopic analysis of the biopsied sterile tissue specimens via immunohistochemical staining, accompanied by the evidence of associated tissue damage<sup>3</sup>; (4) complete clinical data and (5) follow-up possible through the eMRS from admission to discharge or death. In contrast, patients with any of the following criteria were excluded: (1) a possible or probable diagnosis of IPA; (2) a history of IPA prior to pathological diagnosis or chronic cavitary pulmonary aspergillosis; (3) tracheobronchial and allergic bronchopulmonary aspergillosis; (4) lung infection caused by other fungi or pathogens and (5) missing more than a third of clinical data, including those pertaining to clinical characteristics, thoracic imaging and laboratory examinations.

To assess the resolution of the model, a control cohort was established. Patients who had a diagnosis of pneumonia at discharge, with definitive non-fungal aetiologies and were hospitalised during the study were retrieved and matched 1:1 with IPA patients in their respective hospitals, with age ( $\pm 5$  years) and sex as matching variables.

### 2.2 | Data collection

According to guidelines and the literature,<sup>3,4,15</sup> data regarding demographics and clinical characteristic of the patients with IPA and non-fungal pneumonia were collected and entered into electronic case report forms by two recorders. To improve the performance of early diagnosis, only clinical data and chest CT scan taken at the time of presentation for suspected IPA prior to histopathologic diagnosis were used. For patients with multiple hospitalisations, only the data recorded before the first pathological diagnosis of IPA were collected. The CT image findings of lung lesions in both cohorts were sorted by two independent radiologists. Positive *Aspergillus* cultures of lower respiratory secretions were considered eligible for model training and validation as a clinical characteristic if the specimen had  $\leq 10$  squamous cells and  $\geq 25$  white blood cells per low power field or a ratio of squamous cells to white cells of  $< 2.5$ .

### 2.3 | Chest CT image pre-processing

Before model training, image standardisation and resizing method were adopted to eliminate differences in CT images due to different equipment and software used in different medical settings, and to facilitate the recognition of images by the model. All CT images used in this study were tri-channel grey images, that is, each pixel is represented by three numerical values R, G, B and  $R = G = B$ . During

image standardisation, the mean value was subtracted from the R, G and B value for each channel of each CT image and divided by the standard deviation, yielding standardised image outputs. The mean and standard deviation were calculated from the R, G and B values of the CT images in the training set. After that, the standardised images were resized to a fixed  $256 \times 256$  pixel size.

## 2.4 | Deep learning model configuration

The deep learning model, named IPA-NET, consists of three interrelated modules, including the DenseNet121 Network,<sup>16</sup> Feature Concatenation and the Fully Connected Network. Each module contains several computing units consisting of neurons, including the input layer, convolutional layer,<sup>17</sup> pooling layer, batch normalisation layer, rectified linear unit (ReLU) layer, embedding layer, dropout layer and fully connected layer. All of these layers are integrated into IPA-NET to simulate the analytic process similar to that of the human brain, which is capable of being self-taught. Briefly, the first module (the DenseNet121 network) extracts the features of each pre-processed CT image inputted by the Input Layer, convolutes them into a one-dimensional feature vector, and then outputs to the second module (the Feature Concatenation) which receives all clinical features of the same patient imported by the embedding layer, converts them into one-dimensional vectors and concatenates with the CT image feature vector in a sequential order, and forms a new feature vector and outputs to the third module. The third module, the Fully Connected Network, consists of a Fully

Connected Layer and a Dropout Layer. Upon receiving the output of the Feature Concatenation, it identifies and classifies the feature vectors of the data, and then produces and outputs the final results. The results are displayed as IPA or non-IPA (Figure 1).

## 2.5 | Construction of training and test sets

The pre-processed CT images and clinical features including comorbidities, medical history, laboratory examinations and CT image findings of the two cohort patients in the first two hospitals were randomly divided into a training set and an independent internal test set at a ratio of 9:1. An independent external test set was also constructed using patient data from the third hospital for further verification of the model. Since clinical features are binary variables, we assigned a weight of 0 to 'no' and 1 to 'yes'. During dataset construction, each CT image and all clinical features of the same patient were combined and labelled as IPA or non-IPA and allocated to the same subset (Figure 2).

## 2.6 | Model training and verifications

The training process is shown in Figure 1. First, the transfer learning fine-tuning method was used to expand the training data, improve the generalisation ability of the model and prevent overfitting.<sup>7,18</sup> For this purpose, 300,000 single-channel grey chest CT images published on the website of China National Center for

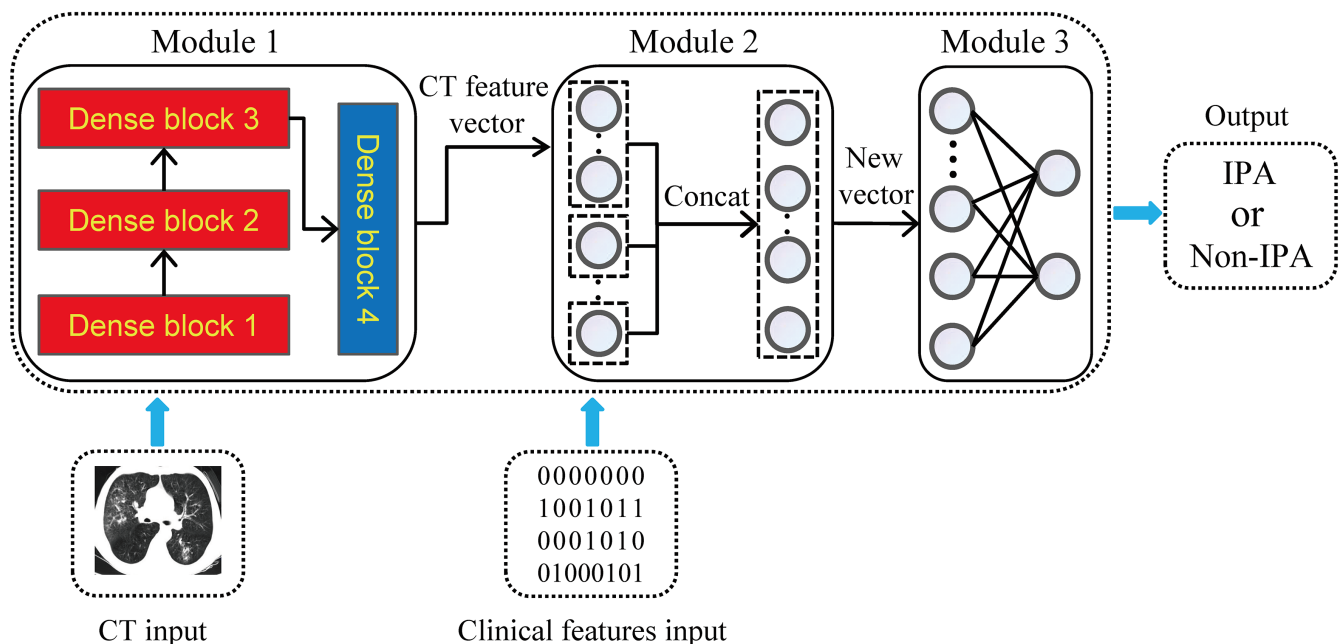


**FIGURE 1** Schematic diagram of the deep learning model. Notes: IPA-NET consists of three interrelated modules and neurons. Module 1 (DenseNet121 Network) extracts and convolutes and outputs CT image feature vector. Module 2 (Feature Concatenation) receives inputted CT image feature vector and clinical features of the same patient and concatenates them sequentially into a new feature vector. Module 3 (Fully Connected Network) receives the output of the second module, classifies the feature vectors of the data and outputs the final results. CT, computed tomography; IPA, invasive pulmonary aspergillosis; The circles inside the modules represent neurons.

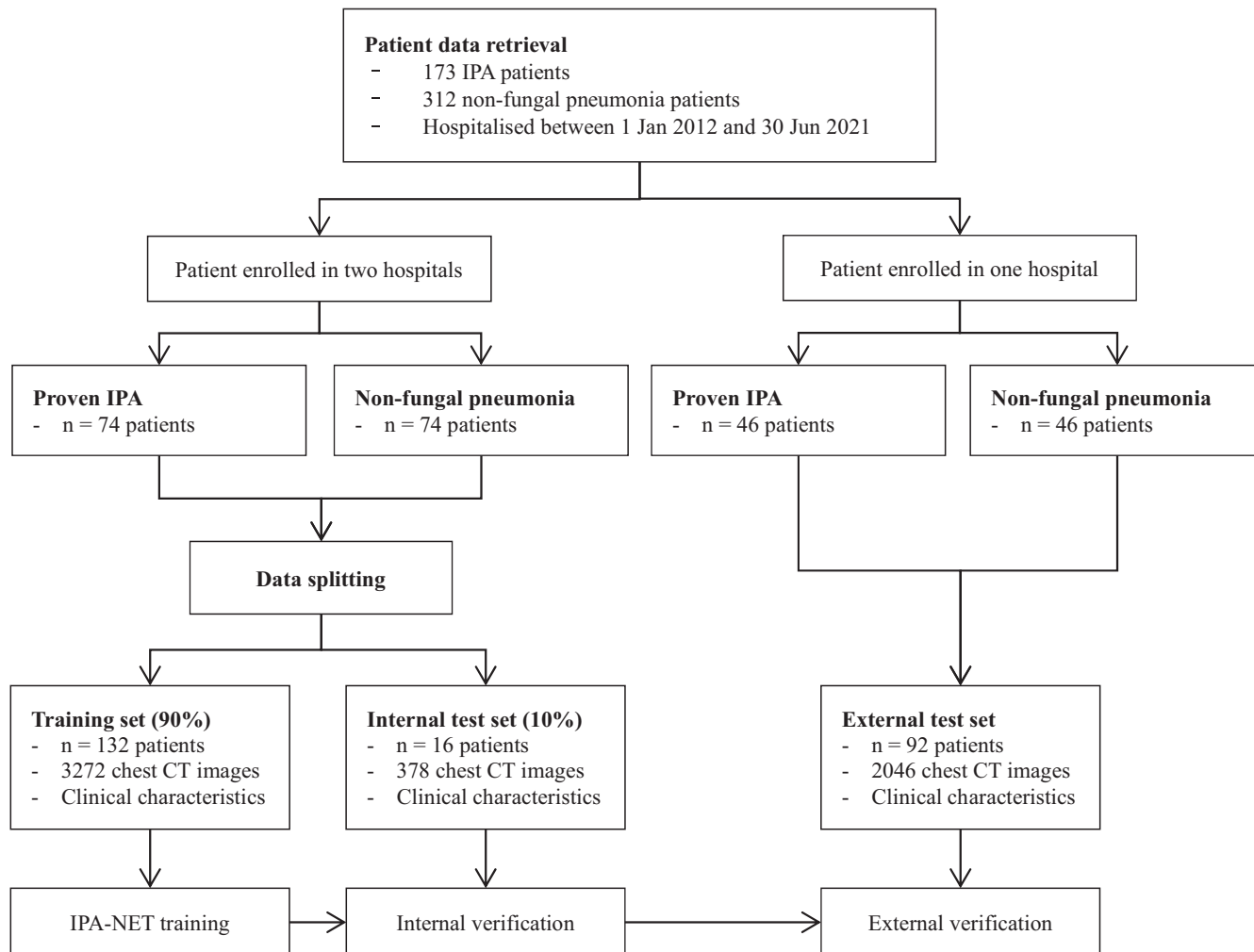


FIGURE 2 Patient enrolment and study flowchart. CT, computed tomography; IPA, invasive pulmonary aspergillosis.

Bioinformation (CNCB),<sup>19</sup> which predominantly consisted of images obtained from patients with bacterial, viral and mycoplasma pneumonia, were converted into tri-channel grey images and used for transfer training of the model, mainly the first three dense blocks of the DenseNet121 network module (the red part in Figure 1). In this way, the deep learning model could master the basic features of the chest CT images in advance. Second, the training set was used to train the fourth dense block of the DenseNet121 network module (blue part in Figure 1) to ensure that the DenseNet121 network masters the CT image features of IPA. While the fourth dense block was being trained, the first three dense blocks were frozen. Third, the Fully Connected Network was trained by the concatenated feature vectors from the second module to generate results.

During the training process, a total of 500 training epochs were completed. In each epoch, the model received a batch of CT images, clinical features and their labels, and produced model parameters. The initial learning rate of training was set to 0.001, which determined the degree of continuous update and automatic adjustment of model parameters. A set of model parameters was generated per 20 training epochs, which was saved and used for the model verification using the internal test set without the labels. The parameters

with the best diagnostic efficacy were selected as the final model parameters and further verified using the external test set.

## 2.7 | Model attention

The deep learning visualisation method was used to generate an attention map to show the suspicious areas identified by IPA-NET that attracted the most attention of the model.<sup>20</sup> A cut-off value of 0.5 was used to preserve the high response of the area suspicious of IPA.

## 2.8 | Performance comparison

First, image feature extraction ability was compared among four convolutional neural network-based deep learning models: DenseNet121, ResNet50, VGG19 and Inception-V3, which were constructed previously for the diagnosis of various diseases.<sup>16,21-23</sup> We employed 1.2 million colour pictures from the ImageNet for transfer learning of the models.<sup>24</sup> Then, these models were further trained and validated using only the chest CT images of the training

and internal test sets. Second, to compare the diagnostic efficacy of IPA-NET with these four deep learning models, IPA-NET (IPA-NET1) was also trained using the same 1.2 million colour pictures for transfer learning, and then trained and validated using both the chest CT images and clinical characteristics of the training and internal test sets. Third, to evaluate the effect of transfer learning on the diagnostic performance, we trained IPA-NET with either 1.2 million colour pictures (IPA-NET1) or the 300,000 chest CT images. Then, these two models were trained and internally validated using both the chest CT images and clinical characteristics.

## 2.9 | Statistical analysis

Continuous variables are presented as means and standard deviations, and discrete variables as frequencies and percentages. The random forest regression method was used to fill in missing clinical data.<sup>25</sup> Variables with large amounts of omitted data (e.g., galactomannan test) were excluded. Accuracy, precision, sensitivity, specificity, area under the receiver operating characteristic curve (AUC) and F1 score, were used to evaluate the diagnostic performance of IPA-NET and expressed as percentages with 95% confidence intervals (CIs).<sup>26</sup> All deep learning methods, statistical analyses, and graphing were performed using the Pytorch toolkit and Python 3.7 (Python Software Foundation, [www.python.org](http://www.python.org)).

## 3 | RESULTS

### 3.1 | Patient enrolment and basal characteristics

A flowchart of patient data retrieval and the study is shown in [Figure 2](#), and the demographics and clinical characteristics of the two cohorts of enrolled patients are shown in [Table 1](#). In the IPA cohort, 44.2% of patients had a history of tuberculosis, whereas in the control cohort, 9.2% had a history of tuberculosis, with bacterial pneumonia accounting for 92.5%, followed by viral pneumonia in 3.3%. Appropriately, 29 clinical characteristics and 6 to 42 CT images of lung lesions were collected from each patient, and the number of CT images in the two groups was comparable.

### 3.2 | Training effect of IPA-NET

During the 500 training epochs of the model training, the diagnostic accuracy of the model gradually increased, while the training loss gradually decreased, and the two curves of accuracy and training loss eventually stabilised. No obvious over-fitting was observed ([Figure 3](#)).

### 3.3 | Model diagnostic efficacy

When tested using the internal test set, IPA-NET showed a diagnostic accuracy of 96.8%, a precision of 0.96, a sensitivity of

0.98, a specificity of 0.96, an AUC of 0.99 (95% CI, 0.98–0.99), and an F1 score of 0.97. When further verified using the external test set, IPA-NET showed an accuracy of 89.7%, a precision of 0.91, a sensitivity of 0.88, a specificity of 0.91, an AUC of 0.95 (95% CI, 0.92–0.95) and an F1 score of 0.89 ([Figure 4](#)).

### 3.4 | Model attention to suspicious lesions

Suspected IPA-related lesions in the CT images detected by IPA-NET are shown in [Figure 5](#). Regardless of whether the internal or external test set was used, the attention maps showed that IPA-NET was able to detect IPA-related lesions and label them as highly responsive areas, indicating that the model can adequately learn the features of chest CT images and respond appropriately.

### 3.5 | Comparison of different models

DenseNet121 shows better image feature extraction ability than other convolutional neural network-based deep learning models. The diagnostic efficacy of IPA-NET1 was superior to that of DenseNet121, and IPA-NET showed the best performance among all models when validated using the internal test set ([Table 2](#)).

## 4 | DISCUSSION

In this study, IPA-NET showed optimal diagnostic performance for IPA, with high accuracy, precision, sensitivity, specificity, AUC and F1 score as verified using the internal or external test sets. It only takes about 10s to make a diagnosis. The relatively large AUCs of the internal and external validations indicate that IPA-NET can identify new CT images and clinical characteristics that have not previously entered the model. The relatively high F1 score shows that the model has good classification ability without over-fitting. Nonetheless, the diagnostic performance of the model declined when validated externally, with more false positives and negatives. This may have occurred because IPA patients in the external test set had fewer clinical characteristics than those in the training set, which might lead to false negatives. In addition, due to insufficient data, the model might fail to distinguish similar CT images and clinical features of IPA in the training set from those of non-fungal pneumonia in the external test set, leading to false positives.

### 4.1 | Visualisation in deep learning

We employed a visualisation technique to show suspicious areas of interest to the model.<sup>20</sup> Once the model determines that the patient has IPA, it tells the clinician which area on the CT image attracts the model's attention the most. Although the CT image manifestations of IPA patients varied, IPA-NET could still detect the suspected regions, including cavities, crescents, multiple nodules and

TABLE 1 Demographic and clinical characteristics of patients with IPA and non-fungal pneumonia.

Variables	From two hospitals		From one chest hospital	
	IPA group (n = 74)	Control group (n = 74)	IPA group (n = 46)	Control group (n = 46)
Age, years; mean ± SD	51.01 ± 13.05	53.5 ± 14.62	50.13 ± 12.85	52.2 ± 13.71
Sex, n (%)				
Male	41 (55.4)	41 (55.4)	36 (78.3)	36 (78.3)
Female	33 (44.6)	33 (44.6)	10 (21.7)	10 (21.7)
Comorbidities, n (%)				
Cancer	17 (23)	14 (18.9)	0 (0)	0 (0)
Hypertension	10 (13.5)	23 (31.1)	5 (10.9)	23 (50)
Diabetes mellitus	15 (20.3)	10 (13.5)	10 (21.7)	0 (0)
COPD	6 (8.1)	5 (6.8)	2 (4.3)	0 (0)
Pulmonary tuberculosis	12 (16.2)	9 (12.2)	41 (89.1)	2 (4.3)
Solid organ transplantation	1 (1.4)	1 (1.4)	0 (0)	0 (0)
Bone marrow transplantation	6 (8.1)	2 (2.7)	0 (0)	0 (0)
Immune disorders	1 (1.4)	3 (4.1)	0 (0)	0 (0)
Calculosis	10 (13.5)	8 (10.8)	7 (15.2)	0 (0)
MODS	3 (4.1)	4 (5.4)	0 (0)	0 (0)
Medical history, n (%)				
Body temperature >38°C	16 (21.6)	12 (16.2)	3 (6.4)	0 (0)
Use of immunosuppressant	9 (12.2)	2 (2.7)	0 (0)	0 (0)
Radiochemotherapy	11 (14.9)	6 (8.1)	0 (0)	0 (0)
Long-term steroid use	8 (10.8)	6 (8.1)	1 (2.2)	2 (4.3)
Long-term use of broad-spectrum antibiotics	44 (59.5)	37 (50)	19 (41.3)	7 (15.2)
Multiple hospitalisations	14 (18.9)	19 (25.7)	6 (13)	0 (0)
History of surgery	21 (28.4)	25 (33.8)	8 (17.4)	0 (0)
Laboratory examination, n (%)				
Neutropenia (<0.5 × 10 <sup>9</sup> /L)	10 (13.5)	5 (6.8)	2 (4.3)	1 (2.2)
Lymphopenia (<1.1 × 10 <sup>9</sup> /L)	42 (56.8)	34 (45.9)	13 (28.3)	0 (0)
Positive G test	12 (16.2)	12 (16.2)	8 (17.4)	0 (0)
Positive <i>Aspergillus</i> culture <sup>a</sup>	17 (23)	1 (1.4)	3 (6.4)	0 (0)
CT image findings, n (%)				
Multiple nodular shadow	53 (71.6)	25 (33.8)	33 (71.7)	2 (4.3)
Cavity sign	27 (36.5)	5 (6.8)	39 (84.8)	0 (0)
Halo sign	1 (1.4)	0 (0)	0 (0)	0 (0)
Air crescent sign	5 (6.8)	0 (0)	2 (4.3)	0 (0)
Subpleural nodules	10 (13.5)	4 (5.4)	0 (0)	0 (0)
Bronchiectasis	29 (39.2)	23 (31.1)	29 (63)	21 (45.7)
Ground glass shadow	15 (20.3)	6 (8.1)	1 (2.2)	0 (0)
Multiple patchy shadows	47 (63.5)	47 (63.5)	40 (87)	44 (96)

Abbreviations: COPD, chronic obstructive pulmonary disease; CT, computed tomography; G test, test for 1,3-β-D glucan antigen detection; IPA, invasive pulmonary aspergillosis; MODS, multiple organ dysfunction syndrome.

<sup>a</sup>Lower respiratory secretion culture.

signs of bronchiectasis, indicating that the model had fully grasped the image features of IPA and was able to make respond appropriately (Figure 5). Although image segmentation is often used in

deep learning to improve model recognition ability, imaging manifestations such as nodules and cavities near the pleura may be segmented. To avoid the segmentation of these manifestations, we

used unsegmented CT images for model training and verification. Consequently, IPA-NET could still detect the suspicious areas in the CT images, without interference from the area outside the lung fields.

## 4.2 | Comparison between IPA-NET and existing models

To the best of our knowledge, IPA-NET is the first deep learning model built for the automatic diagnosis of IPA. When compared with two clinical algorithms, the model showed an improved diagnostic performance. Rozaliyani et al. presented a scoring model with four weighted risk factors that yielded a diagnostic sensitivity of 77.4%, a specificity of 48.4% and an AUC of 0.69 (95% CI, 0.57–0.79).<sup>27</sup> Blot

et al. also proposed a model based on clinical information analysis to distinguish invasive infection from fungal colonisation in critically ill patients with positive *Aspergillus* cultures in secretions from the low respiratory tract, and then validated by biopsy or autopsy. The model showed a sensitivity, specificity and AUC of 92%, 61%, and 0.76 (95% CI, 0.67–0.85), respectively.<sup>28</sup> Compared with these clinical algorithms, our model has the following advantages: (1) IPA-NET employs a hierarchical neural network module to extract features from CT images and clinical characteristics, which might not be detected by the naked eye; (2) CT images and clinical features are readily available before a definitive diagnosis is made, which is conducive to early diagnosis and (3) the diagnostic process is automated and requires no manual intervention.

In the present study, we selected the DenseNet121 network to build IPA-NET, because DenseNet121 has shown better image feature extraction ability among four convolutional neural network-based deep learning models, and IPA-NET (IPA-NET1) showed better diagnostic efficacy when compared with these models (Table 2). The reason might be that IPA-NET1 can concatenate imaging and clinical features so that the model can fully learn the most features of IPA. Besides, the effect of transfer learning using 300,000 chest CT images is better than that obtained using 1.2 million colour pictures; thus, the diagnostic performance of IPA-NET is better than that of IPA-NET1. The reason might be that IPA-NET has acquired the ability to learn low-order features of the chest CT images in the process of transfer learning, which contributes greatly to improving the model performance. When tested using the external test set, IPA-NET still showed good diagnostic and classification performance for unknown data, as shown in Table 2.

Our study had some limitations. First, although the initial results were satisfactory, insufficient data may affect the diagnostic performance of the model. We believe that greater accuracy could be achieved by including more CT images and clinical information for

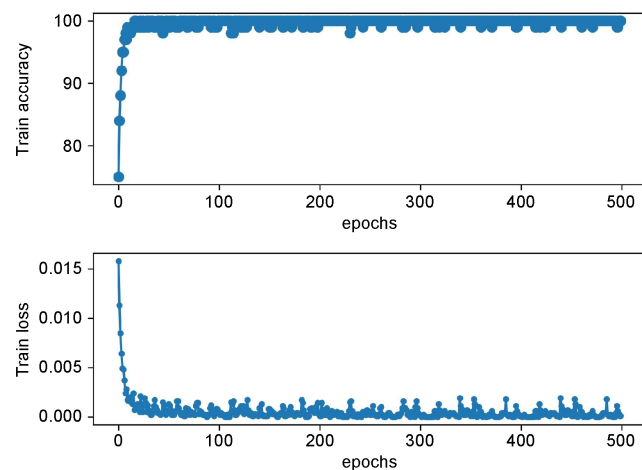


**FIGURE 3** Trends of training loss and accuracy during model training. Note: the diagnostic accuracy of the model gradually increased, while the training loss gradually decreased, and the two curves of accuracy and training loss eventually stabilised during the model training process. No obvious over-fitting was observed.

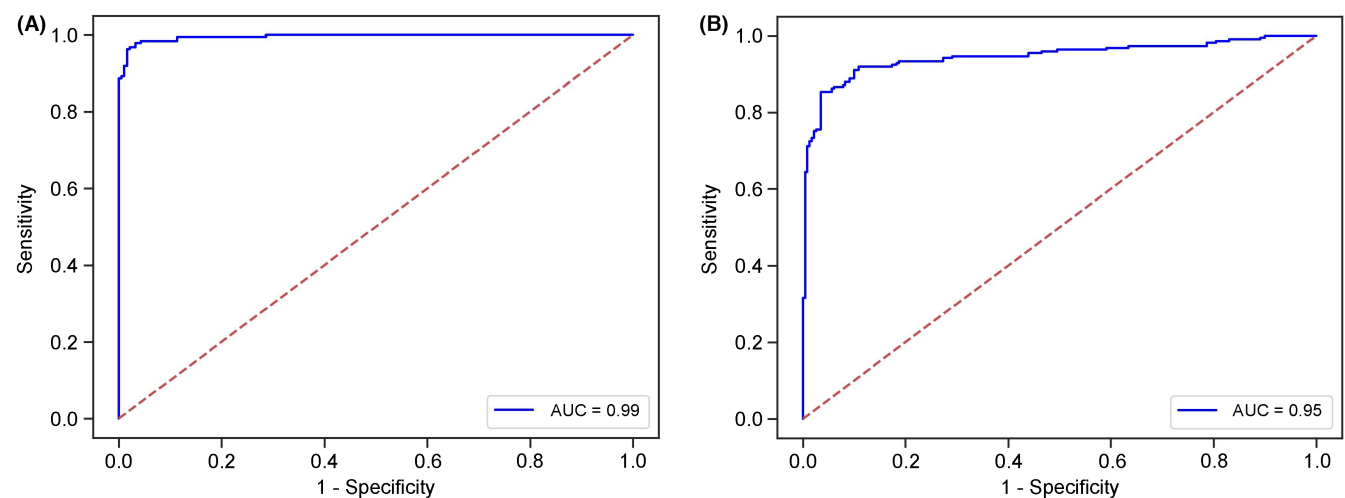


**FIGURE 4** Receiver operating characteristic curves of the efficacy of IPA-NET in diagnosing IPA. Note: the figure indicates the AUCs of IPA-NET validated using the internal test set (A) and external test set (B). While validated using the external test set, the diagnostic performance of the model declined. AUC, area under the curve.

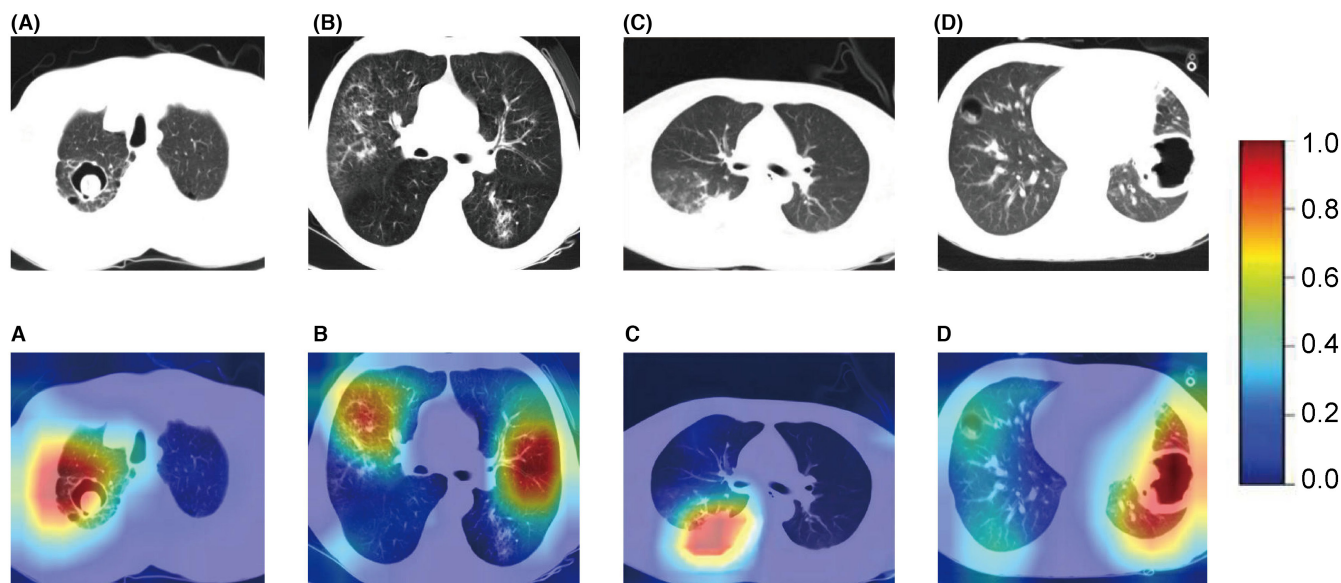


**FIGURE 5** Attention diagram of the deep learning model. Note: Up panel (A–B) and (C–D) show the chest CT features of IPA patients in the internal and external test sets, respectively. As shown in lower panel (A–D), the deep learning model detected regions with suspicious lesions related to IPA in the image. The colour bar on the right panel indicates the intensity of attention, with red indicating the maximum.

Model	Accuracy	Precision	Sensitivity	Specificity	AUC	F1 score
IPA-NET						
Internal verification	96.8%	0.96	0.98	0.96	0.99	0.97
External verification	89.7%	0.91	0.88	0.91	0.95	0.89
IPA-NET1	94.3%	0.93	0.96	0.92	0.99	0.94
DenseNet121	92.9%	0.94	0.92	0.94	0.97	0.93
ResNet50	90.7%	0.90	0.91	0.90	0.97	0.91
Vgg19	90.0%	0.89	0.91	0.89	0.96	0.90
Inception-V3	90.2%	0.92	0.88	0.93	0.95	0.90

**TABLE 2** Comparison of diagnostic efficacy between the IPA-NET and other deep learning models.

Abbreviations: AUC, area under the curve; IPA-NET, transfer learning using 300,000 chest CT images; IPA-NET1, transfer learning using 1.2 million colour pictures from the ImageNet.

model training. Second, due to the retrospective nature of the study, there were considerable missing clinical data. Although a random forest regression algorithm was used to fill in the missing data, the reliability of the results decreased. Third, we did not include patients with non-IPA fungal pneumonia due to insufficient data, which may reduce its clinical applicability. Lastly, patients in the external test set had fewer clinical features than those in the training set, which could be attributed to the fact that the patients were mainly from a tuberculosis specialist hospital. As a result, the false positive and false negative rates increased. However, this misclassification could be improved by expanding the sample size of IPA patients from different hospitals for model training.

In conclusion, IPA-NET provides a non-invasive, objective and reliable method for the early diagnosis of IPA. The diagnosis does not require manual intervention, only chest CT images and clinical features that are readily available in the early stages of the disease,

making it a promising diagnostic tool in different medical settings such as outpatient clinics, wards, and particularly, intensive care units. However, due to the insufficient amount of patient data in the study, the resolution and applicability of the model may be decreased, which needs to be further improved in future studies.

#### AUTHOR CONTRIBUTIONS

Wei Wang involved in conceptualisation (equal); methodology (equal); software (lead); data curation (equal); formal analysis (equal); investigation (equal); visualisation (equal); writing—original draft preparation (equal) and writing—review and editing (equal). Mujiao Li involved in methodology (equal); software (supporting) and writing—original draft preparation (equal). Peimin Fan performed resources (equal); investigation (equal) and validation (equal). Hua Wang involved in conceptualisation (equal); funding acquisition (equal) and writing—review and editing (equal). Jing Cai



performed data curation (equal). Kai Wang performed formal analysis (equal). Tao Zhang involved in Investigation (equal). Zelin Xiao contributed to data curation (equal) and formal analysis (equal). Jingdong Yan performed project administration (equal); resources (equal) and supervision (supporting). Chaomin Chen contributed to funding acquisition (equal); validation (equal) and writing–review and editing (equal). Qingwen Lv performed conceptualisation (equal); methodology (equal); project administration (equal); resources (equal); supervision (lead); validation (equal); visualisation (equal); writing–original draft preparation (equal) and writing–review and editing (equal).

## ACKNOWLEDGEMENT

We wish to thank all of the medical staff of the School of Biomedical Engineering of Southern Medical University, and the departments of radiology in Zhujiang and Nanfang Hospitals, for their assistance with clinical data collection and CT image classification. We also thank Chongyang Duan, MD, Department of Biostatistics, School of Public Health, Southern Medical University for the support and work on data processing and statistical analysis.

## FUNDING INFORMATION

Funding from the National Key R&D Program of China (grant number: 2019YFC0118805), and the Clinical Research Startup Program of Southern Medical University by High-level University Construction Funding of Guangdong Provincial Department of Education (grant number: LC2016PY036) are gratefully acknowledged.

## CONFLICT OF INTEREST

The authors declare no conflict of interest.

## DATA AVAILABILITY STATEMENT

The data that support the findings of this study are available on request from the corresponding authors.

## ORCID

Wei Wang  <https://orcid.org/0000-0002-8984-6795>

Hua Wang  <https://orcid.org/0000-0002-2869-9488>

Jing Cai  <https://orcid.org/0000-0002-7699-3446>

## REFERENCES

- Thompson GR 3rd, Young JH. *Aspergillus* infections. *N Engl J Med*. 2021;385:1496–1509.
- Dignani MC. Epidemiology of invasive fungal diseases on the basis of autopsy reports. *F1000Prime Rep*. 2014;6:81.
- Ullmann AJ, Aguado JM, Arian-Akdagli S, et al. Diagnosis and management of *Aspergillus* diseases: executive summary of the 2017 ESCMID-ECMM-ERS guideline. *Clin Microbiol Infect*. 2018;24(Suppl 1):e1–e38.
- Patterson TF, Thompson GR 3rd, Denning DW, et al. Executive summary: practice guidelines for the diagnosis and management of aspergillosis: 2016 update by the Infectious Diseases Society of America. *Clin Infect Dis*. 2016;63:433–442.
- Jenks JD, Mehta SR, Taplitz R, Aslam S, Reed SL, Hoenigl M. Point-of-care diagnosis of invasive aspergillosis in non-neutropenic patients: *Aspergillus* galactomannan lateral flow assay versus *Aspergillus*-specific lateral flow device test in bronchoalveolar lavage. *Mycoses*. 2019;62:230–236.
- von Eiff M, Roos N, Schulten R, Hesse M, Zühlsdorf M, van de Loo J. Pulmonary aspergillosis: early diagnosis improves survival. *Respiration*. 1995;62:341–347.
- Esteva A, Kuprel B, Novoa RA, et al. Dermatologist-level classification of skin cancer with deep neural networks. *Nature*. 2017;542:115–118.
- Yao Z, Li J, Guan Z, Ye Y, Chen Y. Liver disease screening based on densely connected deep neural networks. *Neural Netw*. 2020;123:299–304.
- Pacal I, Karaboga D, Basturk A, Akay B, Nalbantoglu U. A comprehensive review of deep learning in colon cancer. *Comput Biol Med*. 2020;126:104003.
- Gao XW, Hui R, Tian Z. Classification of CT brain images based on deep learning networks. *Comput Methods Programs Biomed*. 2017;138:49–56.
- Ausawalaithong W, Thirach A, Marukat S, Wilaiprasitporn T. Automatic lung cancer prediction from chest X-ray images using the deep learning approach. *Proceedings of 11th Biomedical Engineering International Conference (BMEiCON'18)*. IEEE; 2018:1–5.
- Elshennawy NM, Ibrahim DM. Deep-pneumonia framework using deep learning models based on chest X-ray images. *Diagnostics*. 2020;10:649.
- Wang S, Kang B, Ma J, et al. A deep learning algorithm using CT images to screen for Corona virus disease (COVID-19). *Eur Radiol*. 2021;31:6096–6104.
- Ibrahim DM, Elshennawy NM, Sarhan AM. Deep-chest: multi-classification deep learning model for diagnosing COVID-19, pneumonia, and lung cancer chest diseases. *Comput Biol Med*. 2021;132:104348.
- Prasad A, Agarwal K, Deepak D, Atwal SS. Pulmonary aspergillosis: what CT can offer before it is too late! *J Clin Diagn Res*. 2016;10:TE01–TE05.
- Huang G, Liu Z, Van Der Maaten L, Weinberger KQ. Densely connected convolutional networks. *Proceedings of 2017 IEEE Conference on Computer Vision and Pattern Recognition (CVPR)*. IEEE; 2017:2261–2269.
- LeCun Y, Boser B, Denker JS, et al. Backpropagation applied to handwritten zip code recognition. *Neural Comput*. 1989;1:541–551.
- Keremany DS, Goldbaum M, Cai W, et al. Identifying medical diagnoses and treatable diseases by image-based deep learning. *Cell*. 2018;172:1122–1131.e9.
- Zhang K, Liu X, Shen J, et al. Clinically applicable AI system for accurate diagnosis, quantitative measurements, and prognosis of COVID-19 pneumonia using computed tomography. *Cell*. 2020;182:1360.
- Selvaraju RR, Cogswell M, Das A, Vedantam R, Parikh D, Batra D. Grad-CAM: visual explanations from deep networks via gradient-based localization. *Int J Comput Vis*. 2020;128:336–359.
- He K, Zhang X, Ren S, Sun J. Deep residual learning for image recognition. *Proceedings of 2016 IEEE Conference on Computer Vision and Pattern Recognition (CVPR)*. IEEE; 2016:770–778.
- Simonyan K, Zisserman A. *Very deep convolutional networks for large-scale image recognition*. arXiv; 2014:1409.1556 [cs.CV]. doi:10.48550/arXiv.1409.1556.
- Szegedy C, Vanhoucke V, Ioffe S, Shlens J, Wojna Z. Rethinking the inception architecture for computer vision. *Proceedings of 2016 IEEE Conference on Computer Vision and Pattern Recognition (CVPR)*. IEEE; 2016:2818–2826.
- Krizhevsky A, Sutskever I, Hinton GE. ImageNet classification with deep convolutional neural networks. *Proceedings of 26th Annual Conference on Neural Information Processing Systems (NIPS'12)*. Curran Associates Inc; 2013:1097–1105.
- Stekhoven DJ, Buhlmann P. MissForest—non-parametric missing value imputation for mixed-type data. *Bioinformatics*. 2012;28:112–118.

26. Powers DMW. Evaluation: from precision, recall and F-measure to ROC, informedness, markedness and correlation. *Int J Mach Learn Technol.* 2011;2:37-63.
27. Rozaliyani A, Sedono R, Jusuf A, et al. A novel diagnosis scoring model to predict invasive pulmonary aspergillosis in the intensive care unit. *Saudi Med J.* 2019;40:140-146.
28. Blot SI, Taccone FS, Van den Abeele A-M, et al. A clinical algorithm to diagnose invasive pulmonary aspergillosis in critically ill patients. *Am J Respir Crit Care Med.* 2012;186:56-64.

**How to cite this article:** Wang W, Li M, Fan P, et al. Prototype early diagnostic model for invasive pulmonary aspergillosis based on deep learning and big data training. *Mycoses.* 2022;00:1-10. doi: [10.1111/myc.13540](https://doi.org/10.1111/myc.13540)